Supporting Information

Unravelling the Intrinsic Reactivity and Colloidal Instability in Tin-Based Halide Perovskite Precursor Solutions

Jorge Pascual,[*,#,a] *Marion Flatken,*[#,b] *Eros Radicchi,*[c] *Mahmoud Aldamasy,*[b] *Shuaifeng Hu,*[*,d] *Omar E. Solis,*[e] *Silver-Hamill Turren-Cruz,*[e] *Guixiang Li,*[f] *Armin Hoell,*[b] *Susan Schorr,*[b] *Meng Li,*[g] *Filippo De Angelis,*[h,i] *Artem Musiienko,*[b] *André Dallmann,*[j] *Antonio Abate*[*,b,k,l]

[a] Polymat, University of the Basque Country UPV/EHU, 20018 Donostia-San Sebastian, Spain

[b] Helmholtz-Zentrum Berlin für Materialien und Energie, Hahn-Meitner-Platz 1, 14109 Berlin, Germany

[c] Department of Engineering DIMI, University of Verona, Strada Le Grazie 15, 37134, Verona, Italy

[d] Clarendon Laboratory, Department of Physics, University of Oxford, Oxford, UK

[e] Instituto Universitario de Ciencia de los Materiales (ICMUV), Universitat de València, Paterna, Spain

[f] School of Materials Science and Engineering, Southeast University, Nanjing, Jiangsu, 211189 China

[g] Key Lab for Special Functional Materials, Ministry of Education, National & Local Joint Engineering Research Center for High-efficiency Display and Lighting Technology, School of

Materials Science and Engineering, and Collaborative Innovation Center of Nano Functional Materials and Applications, Henan University, Kaifeng 475004, China

[h] Department of Chemistry, Biology and Biotechnology, University of Perugia, Via Elce di Sotto 8, 06123, Perugia, Italy

[i] SKKU Institute of Energy Science and Technology (SIEST), Sungkyunkwan University, Suwon 440-746, South Korea

[j] Humboldt Universität zu Berlin, Institut für Chemie, AG NMR, Germany

[k] Department of Chemical Materials and Industrial Production Engineering, University of Naples Federico II, Piazzale Tecchio 80, Napoli, Italy

[l] Department of Chemistry Bielefeld University, Universitätsstraße 25, Bielefeld, 33615, Germany

Experimental procedure

Materials

SnI_2 and PbI_2 was purchased from TCI and formamidinium iodide (FAI) from Dyenamo. Dimethyl sulfoxide (DMSO), *N*,*N*-dimethylformamide (DMF), DMSO-d6, and DMF-d7 were purchased from Sigma-Aldrich.

Solution preparation

Solutions were prepared by preparing a stock solution of the metal halide, adding it to FAI powder, and adding the corresponding solvent volume after recalculating the concentration. Solutions at different concentrations were obtained by preparing the most concentrated one and diluting it accordingly. The solutions and samples for characterization were prepared inside a N_2-filled glove box.

Characterization methods

Interpretation of ^{119}Sn and ^{207}Pb-NMR data

This technique enables direct probing of the Sn^{2+} and Pb^{2+} environments, providing insights into how different ligands and solution components influence the metal centers and their species through their chemical shift values. A downfield shift (higher values, deshielded) indicates reduced electronic density around the metal, while an upfield shift (lower values, shielded) suggests increased electronic density. By correlating these shifts with solvent properties, we infer that a higher chemical shift (deshielded) corresponds to an increased iodide-metal coordination and a more pre-arranged perovskite precursor solution, whereas a lower chemical shift (shielded) implies stronger solvation and a reduced precursor organization. Furthermore, NMR can analyze solutions at the high concentrations relevant to practical applications, unlike other conventional techniques such as UV-vis.

We plotted ^{119}Sn- and ^{207}Pb-NMR data together in the same graph for practical reasons, though it is worth noting that chemical shifts are not comparable in between different nuclei.

Liquid-state ^{119}Sn-NMR

The spectra were all acquired on a Bruker AVII 400 MHz or Bruker AVIII 500 MHz equipped with room-temperature TBO or BBO-probe heads respectively. Typically, a sweep width of 504.3 ppm was used and 64k points were acquired, resulting in a total acquisition time of 435.81 ms. The center frequency had to be adjusted from sample to sample to detect the desired

signal, therefore, on new samples, a full scan of the possible shift range was acquired (1000 to -3000ppm). We used a 30° pulse in order to minimize the recycle delay down to 2 s. The number of scans thus ranged from 128 for very concentrated samples to 16k scans for very diluted samples.

Liquid-state ^{207}Pb-NMR

The spectra were acquired on a Bruker AVII 400 MHz or Bruker AVIII 500 MHz equipped with room temperature TBO or BBO-probe heads respectively. Typically, a sweep width of 897 ppm was used, and 8192 points were acquired, resulting in a total acquisition time of 54.48 ms. The center frequency had to be adjusted from sample to sample to detect the desired signal. We used a 30° pulse to minimize the recycle delay to 200 ms. All other spectra were measured with standardized parameter sets from Bruker Topspin version 2.1 (AV400) and 3.0 (AV500).

The spectra presented differences in the signal-to-noise ratio, thus the higher noise in some of the spectral baselines, particularly for the solutions with the lowest concentrations. All existing signals in all spectra were identified and pointed out. For our specific sample comparison using the same halide, we ruled out any significant influence on the conclusions from relativistic effects coming from the presence of large nuclei.[1]

Density Functional Theory (DFT) calculations

Density functional theory (DFT) calculations on SnI_2, PbI_2, $FASnI_3$ and $FAPbI_3$ solvated systems were run using the Gaussian 09 software package.[2] Geometry optimization was done employing the B3LYP exchange–correlation functional[3-4] and Grimme's van der Waals dispersion interactions DFT-D3,[5] simulating solvents both with an implicit solvation model (polarizable continuum model, PCM)[6] and adding one explicit solvent molecule in the case of the solvated systems. Mixed basis sets were adopted, employing 6-31G* for the formamidinium ion (FA^+), DMSO and DMF solvent molecules (i.e., C, H, N, O, S atoms), while for Pb, Sn and I atoms we used the LANL2DZ/LANL2 basis sets/pseudopotentials.

Small Angle X-Ray Scattering (SAXS)

The SAXS measurement has been conducted at the four crystal monochromator X-ray beamline in the laboratory of PTB (Physikalisch-Technische Bundesanstalt) at BESSYII using its synchrotron radiation.[7] The HZB SAXS instrument is equipped with a windowless Dectris 1M PILATUS2 in-vacuum hybrid-pixel detector and an about 3 m long adjustable structure

with a long edge-welded bellow system, which enables to cover various sample to detector distances.[8] The data of this work was collected using two different distances (0.8 m and 3.7 m) at photon energies of 10 keV and 8 keV, respectively. In consequence, the experiment covered a q-range from 0.05 nm^{-1} to 8.5 nm^{-1} (size range of 125.6 nm to 0.74 nm in real space). For the precursor solution data collection an acquisition time of 400 s was selected with three repetitions for the short distance and long distance to achieve good quality data (despite the relatively low sample transmission) and to track potential changes of the specimen over time (which, thus, was excluded). Especially thin (0.1 mm) rectangular borosilicate cuvettes (with a wall thickness of 0.1 mm) purchased from CM Scientific, UK were used. The total flux on the sample has been determined for each energy using a low-scatter pinhole of germanium 500 µm in diameter. At 8 keV, long distance (3.7 m) we indicated 4.8x109 photons/s; respectively, at 10 keV, for the short distance (0.8 m) 2.6x109 photons/s.

Data reduction and radial averaging & fitting: For data reduction the 1D scattering pattern the BerSAS software was used, an advanced version of the BerSAS software[9] applicable for SAXS and SANS. All SAXS curves of the investigated samples were fitted with the program SASfit.[10]

Metal halide perovskites consist of colloidal particles that interact in solution, gradually evolving into crystal nucleation and growth and thus determining the thin film formation.[11-14] However, the colloidal characteristics of tin halide perovskites remain relatively underexplored, with other techniques presenting limitations. Here, SAXS provides in-depth understanding on the nature and interactions of colloidal particles in metal halide perovskite solutions. In previous works we have used the monodisperse Percus-Yevick approximation for hard spheres, which has been proven itself to be suitable to describe iodidoplumbates fairly well. However, in this work we simply refer to the mean distance observed between two centers of mass, reflected in the position of the structure factor peak maximum. This inter-particle distance is not to be equalized to radius/size of the particles.

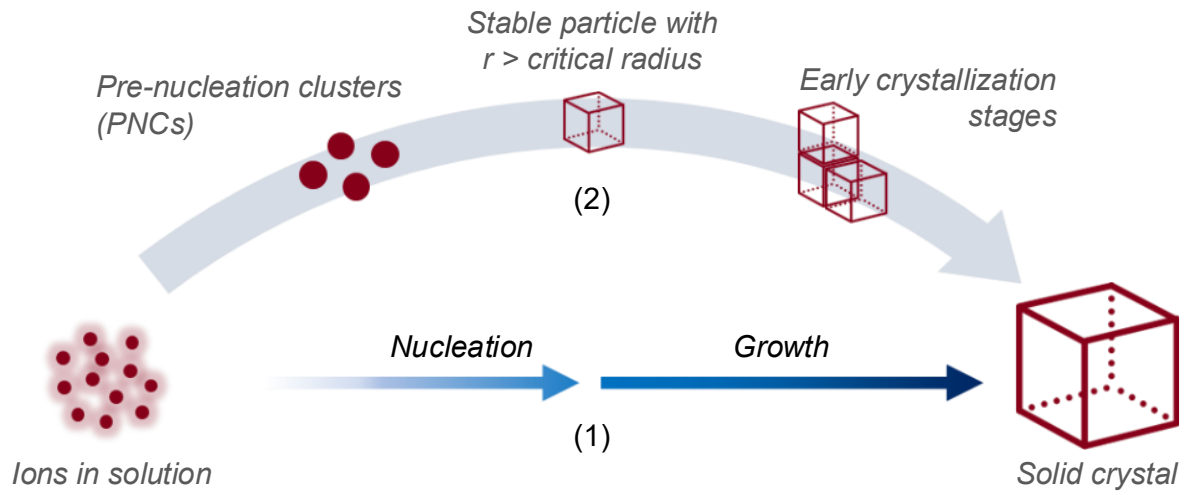

Figure S1. Schematic illustration of the pre-crystallization and early crystallization stages. In the pre-crystallization stage (left), solvated ions in solution undergo short-range organization to form pre-nucleation clusters (PNCs). These PNCs can follow multiple pathways towards crystallization in the framework of non-classical nucleation theory (2), in contrast to crystallization based on classical nucleation theory, which assumes the direct formation and growth of a critical nucleus from monomeric species (1). These dynamically associated species exhibit collective behavior, rather than isolated solvated complexes, but remain below the critical nucleus size. Upon reaching the critical radius (r > critical radius), stable nuclei are formed, marking the onset of the early crystallization stage. Subsequent growth lead to the formation of a solid crystalline phase (right). The scheme distinguishes between solution-state organization prior to nucleation (pre-crystallization stages) and post-nucleation crystal growth (early crystallization stages).

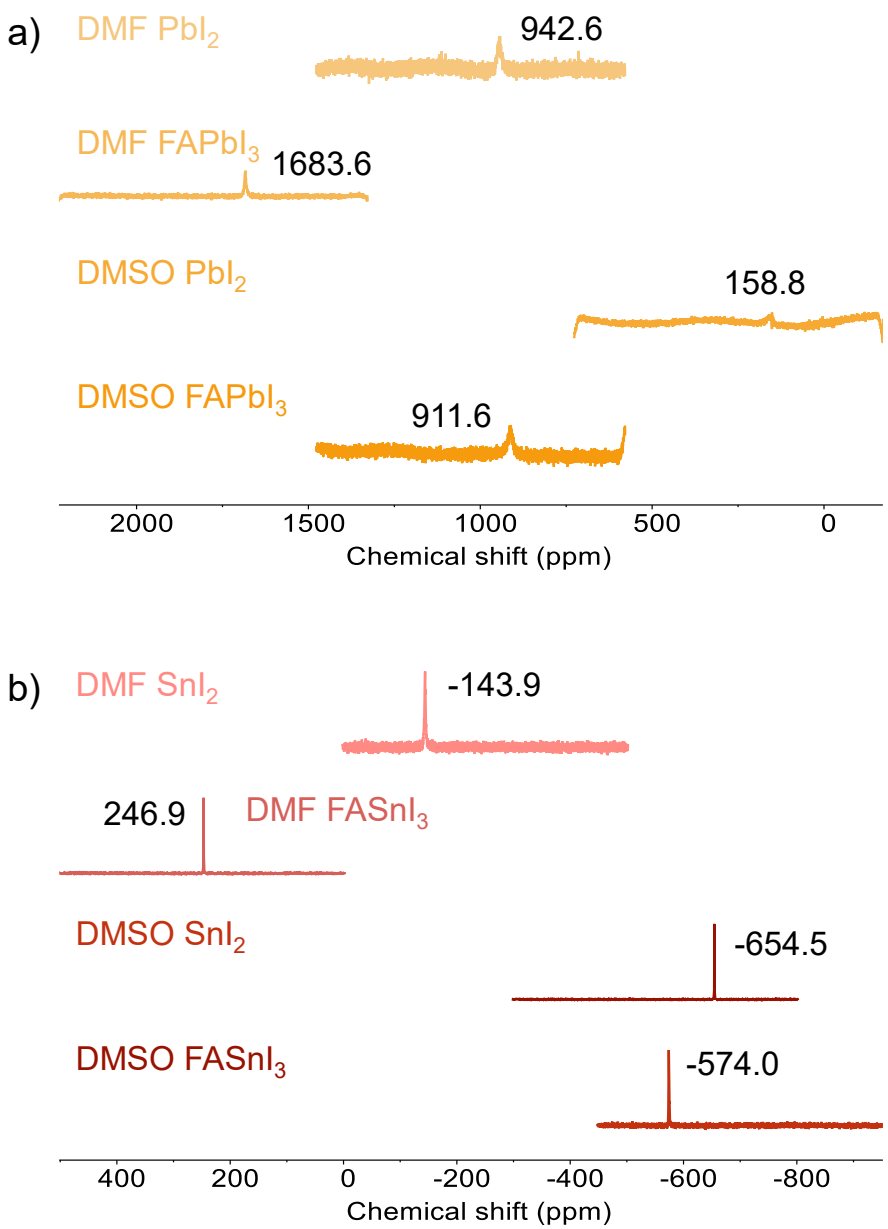

Figure S2. a) ^{207}Pb-NMR spectra of PbI_2 and $FAPbI_3$ in DMF and DMSO at 1 M and b) ^{119}Sn-NMR spectra of SnI_2 and $FASnI_3$ in the same conditions. Figure 1a displays the chemical shift values in here. The ^{207}Pb-NMR spectra have a lower signal-to-noise ratio due to the lower sensitivity of this nucleus.

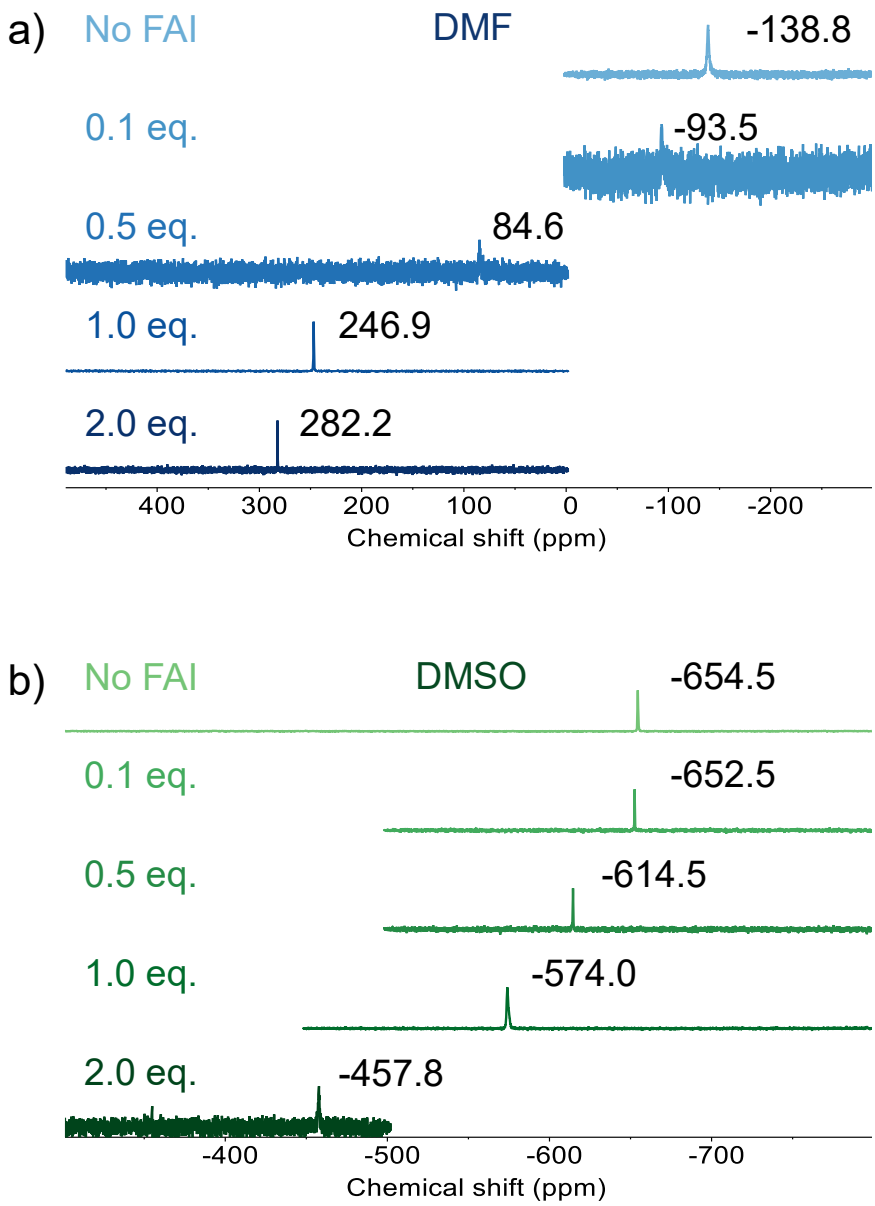

Figure S3. a) ^{119}Sn-NMR of SnI_2 solutions with varying equivalents of FAI in DMF and b) DMSO. Figure 1b displays the chemical shift values in here.

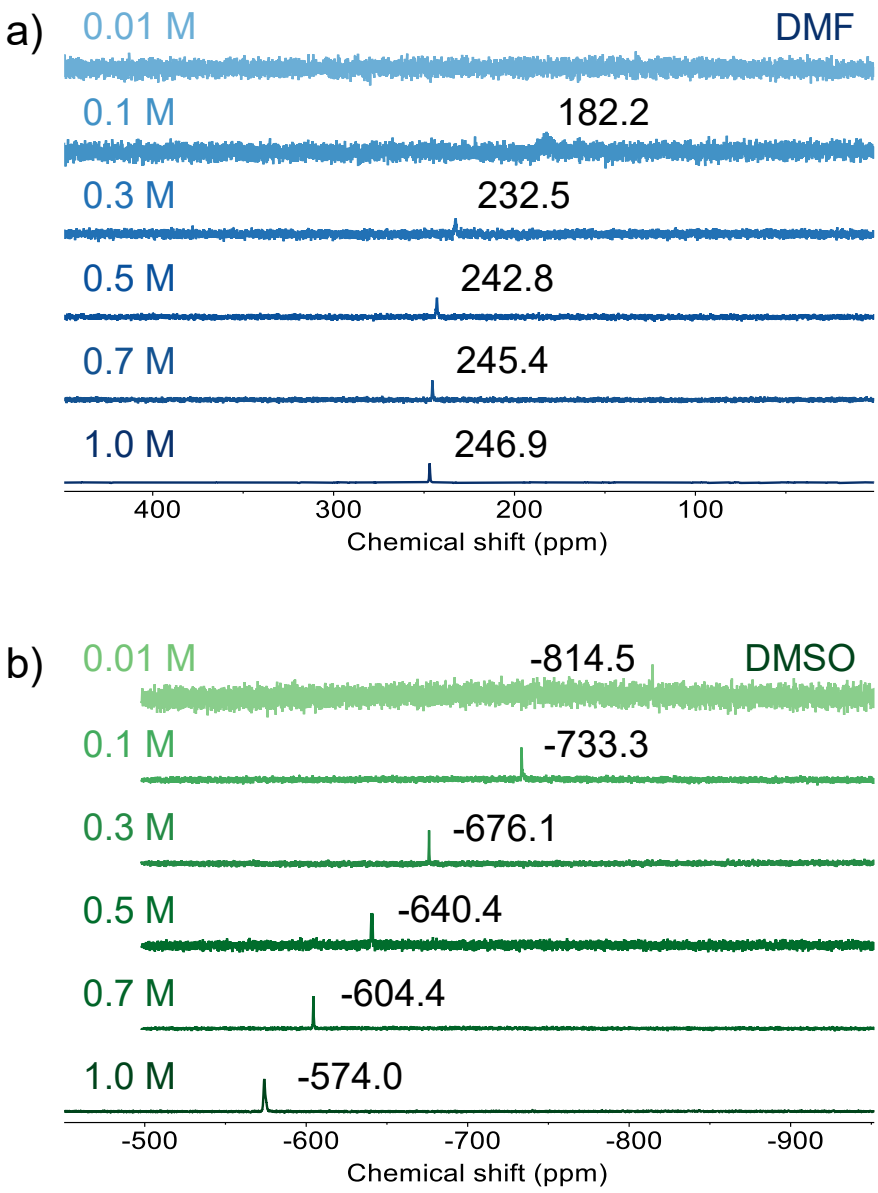

Figure S4. a) ^{119}Sn-NMR spectra of $FASnI_3$ at varying solution concentrations in DMF and b) DMSO. We could not distinguish any signal for 0.01 M sample in DMF despite the long recording time. Figure 1c displays the chemical shift values in here.

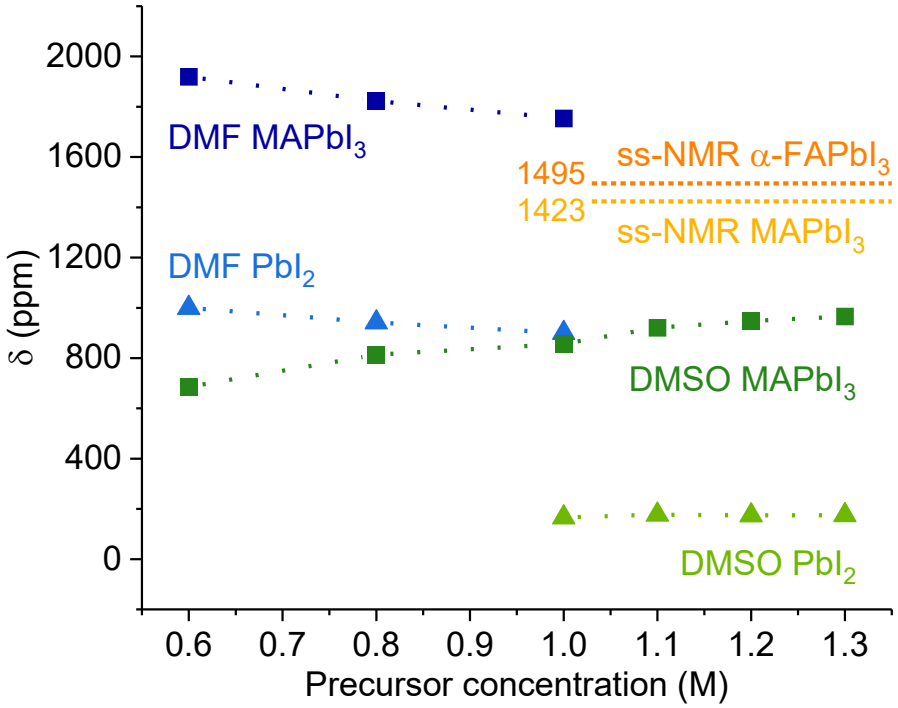

Figure S5. Chemical shift of Pb precursors in DMF and DMSO at different concentrations. The plot shows data from our previous works by Flatken et al. that was adapted to the new reference $Pb(NO_3)_2$ in D_2O at 1.0 M of -2961.2 ppm[12] and from Radicchi et al.[15]

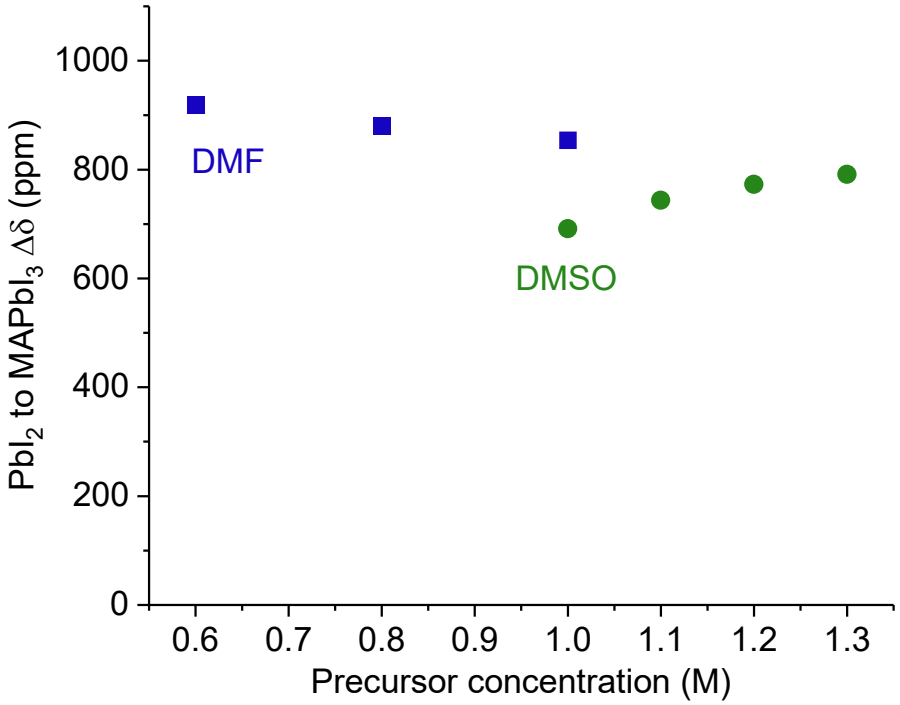

Figure S6. Change in chemical shift from PbI_2 to $MAPbI_3$ from Figure S4.

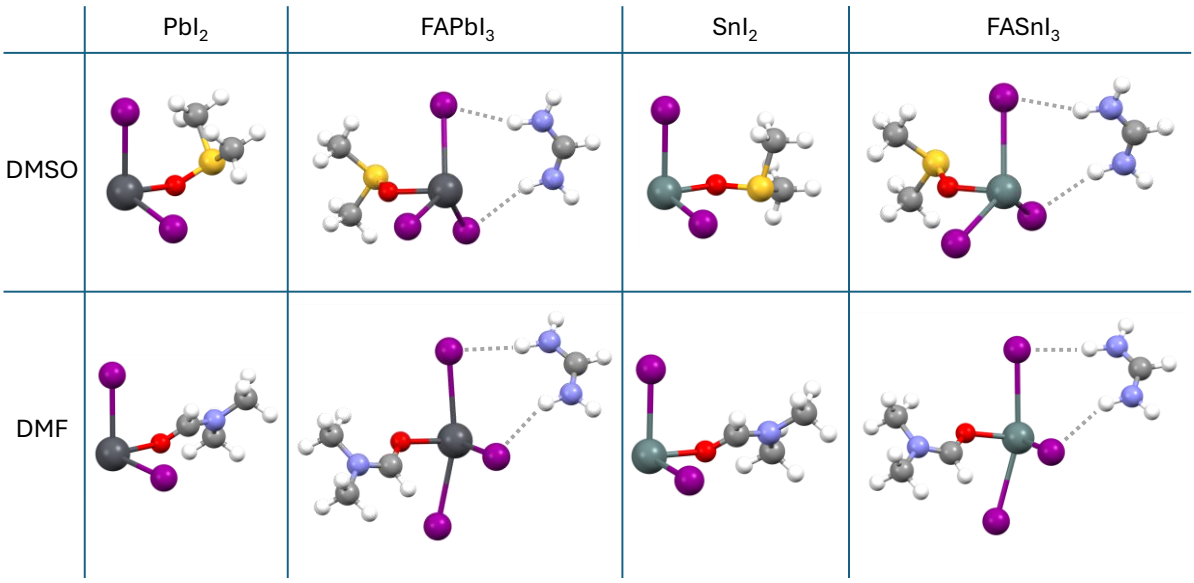

Figure S7. Optimized geometries of PbI_2/$FAPbI_3$ and SnI_2/$FASnI_3$ models coordinated by one solvent (DMSO, DMF) molecule.

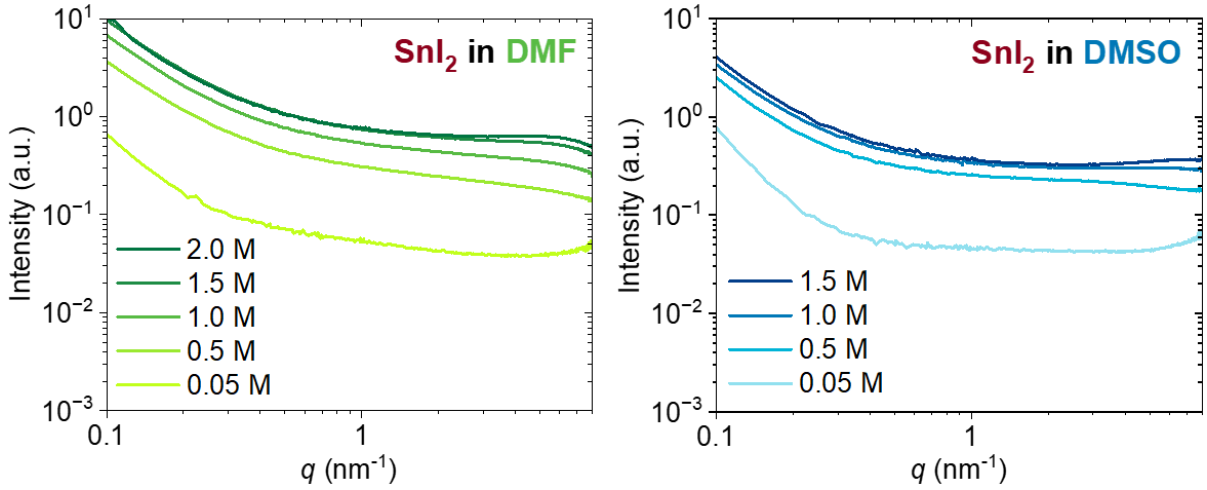

Figure S8. a) SAXS patterns of SnI_2 solutions at varying solution concentrations in DMF and b) DMSO

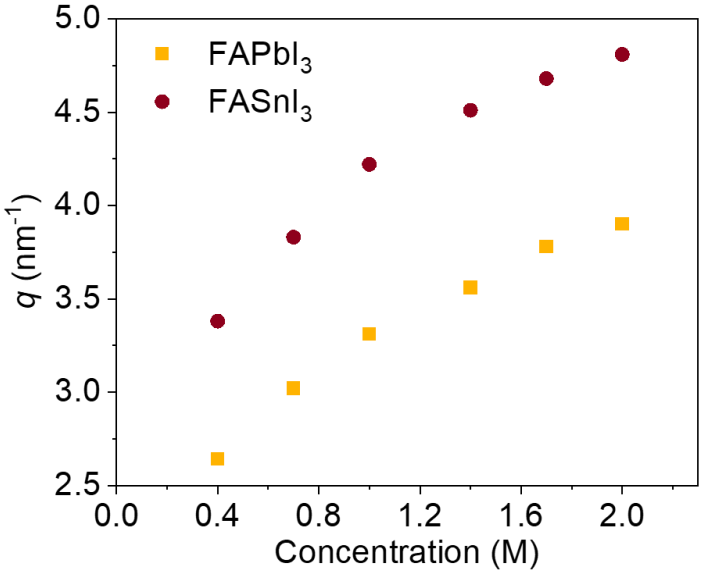

Figure S9. Extracted *q* values from structure factor maxima in SAXS patterns of $FASnI_3$ and $FAPbI_3$ solutions in DMF.

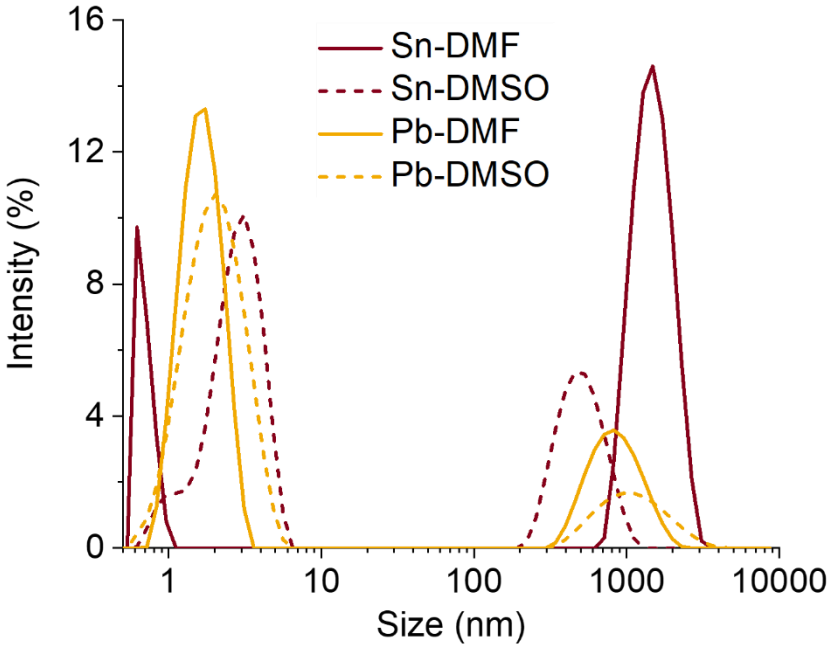

Figure S10. DLS size distribution data for $FASnI_3$ and $FAPbI_3$ solutions at 1 M in DMF and DMSO. Particle size distributions are broader for Sn-based solutions, with much higher contributions of larger entities. DMF shows higher intensities at larger sizes, and DMSO exhibits an increase in the size of smaller particles. DLS results align with SAXS patterns on the higher tendency of Sn-based solutions to agglomerate; the existence of PNCs confirms that both Sn and Pb precursor solutions have colloidal characteristics and thus follow non-classical nucleation pathways.

Table S1. ^{119}Sn-NMR chemical shift of $FASnI_3$ solutions in DMF and DMSO in a concentration range and varying FAI/SnI_2 ratios.

Composition	**Solvent**	**Concentration (M)**	**Chemical shift (ppm)**
$FASnI_3$	DMF	0.1	182.2
$FASnI_3$	DMF	0.3	232.5
$FASnI_3$	DMF	0.5	242.8
$FASnI_3$	DMF	0.7	245.4
$FASnI_3$	DMF	1.0	246.9
$FASnI_3$	DMSO	0.01	-814.5
$FASnI_3$	DMSO	0.1	-733.3
$FASnI_3$	DMSO	0.3	-676.1
$FASnI_3$	DMSO	0.5	-640.4
$FASnI_3$	DMSO	0.7	-604.4
$FASnI_3$	DMSO	1.0	-574.0
$FA_{0.1}SnI_3$	DMF	1.0	-93.5
$FA_{0.5}SnI_3$	DMF	1.0	84.6
$FA_{2.0}SnI_3$	DMF	1.0	282.2
$FA_{0.1}SnI_3$	DMSO	1.0	-652.5
$FA_{0.5}SnI_3$	DMSO	1.0	-614.5
$FA_{2.0}SnI_3$	DMSO	1.0	-457.8

Table S2. ^{119}Sn-NMR chemical shift of SnI_2 solutions in DMF and DMSO in a concentration range, from our previous work.[16]

Composition	Solvent	Concentration (M)	Chemical shift (ppm)
SnI_2	DMF	0.1	-163.7
SnI_2	DMF	0.2	-149.6
SnI_2	DMF	0.3	-145.1
SnI_2	DMF	0.4	-144.2
SnI_2	DMF	0.5	-143.0
SnI_2	DMF	0.6	-140.7
SnI_2	DMF	0.7	-142.4
SnI_2	DMF	0.8	-143.0
SnI_2	DMF	0.9	-143.6
SnI_2	DMF	1.0	-143.9
SnI_2	DMF	1.1	-144.1
SnI_2	DMF	1.2	-146.7
SnI_2	DMSO	0.01	-830.7
SnI_2	DMSO	0.05	-781.4
SnI_2	DMSO	0.1	-757.7
SnI_2	DMSO	0.2	-732.3
SnI_2	DMSO	0.3	-715.2
SnI_2	DMSO	0.4	-702.4
SnI_2	DMSO	0.5	-692.0
SnI_2	DMSO	0.6	-682.9
SnI_2	DMSO	0.7	-675.4
SnI_2	DMSO	0.8	-667.9
SnI_2	DMSO	0.9	-660.4
SnI_2	DMSO	1.0	-654.5
SnI_2	DMSO	1.1	-648.1
SnI_2	DMSO	1.2	-641.8

Table S3. ^{207}Pb-NMR chemical shift of Pb-based reference precursor solutions at 1 M in DMF and DMSO.

Composition	**Solvent**	**Concentration (M)**	**Chemical shift (ppm)**
PbI_2	DMF	(partially dissolved)	942.6
$FAPbI_3$	DMF	1.0	1683.6
PbI_2	DMSO	1.0	158.8
$FAPbI_3$	DMSO	1.0	911.6

Table S4. ^{207}Pb-NMR chemical shift of PbI_2 and $FAPbI_3$ solutions in DMF and DMSO in a concentration range, from our previous works.[12, 15]

Composition	Solvent	Concentration (M)	Chemical shift (ppm)
PbI_2	DMF	0.6	999.8
PbI_2	DMF	0.8	941.8
PbI_2	DMF	1.0	899.8
PbI_2	DMSO	1.0	166.2
PbI_2	DMSO	1.1	177.0
PbI_2	DMSO	1.2	174.6
PbI_2	DMSO	1.3	174.8
$MAPbI_3$	DMF	0.6	1919.4
$MAPbI_3$	DMF	0.8	1822.7
$MAPbI_3$	DMF	1.0	1753.9
$MAPbI_3$	DMSO	0.6	685.6
$MAPbI_3$	DMSO	0.8	813.8
$MAPbI_3$	DMSO	1.0	857.3
$MAPbI_3$	DMSO	1.1	920.6
$MAPbI_3$	DMSO	1.2	947.3
$MAPbI_3$	DMSO	1.3	965.8

Table S5. Extracted q values and calculated d values from SAXS patterns of $FASnI_3$ and $FAPbI_3$ solutions in DMF.

Composition	**Concentration (M)**	q **(nm^{-1})**	d **(nm)**
$FAPbI_3$	2	4.8	1.31
	1.7	4.7	1.34
	1.4	4.5	1.39
	1	4.2	1.49
	0.7	3.8	1.64
	0.4	3.4	1.86
$FASnI_3$	2	3.9	1.61
	1.7	3.8	1.66
	1.4	3.6	1.76
	1	3.3	1.90
	0.7	3.0	2.08
	0.4	2.6	2.38

References

[1] A. Bagno, G. Casella, G. Saielli, *Journal of Chemical Theory and Computation* **2006**, *2*, 37–46.

[2] M. J. Frisch, G. W. Trucks, H. B. Schlegel, G. E. Scuseria, M. A. Robb, J. R. Cheeseman, et al., **2016**, Gaussian 16 Rev. C.01. Wallingford, CT.

[3] A. D. Becke, *The Journal of Chemical Physics* **1993**, *98*, 5648–5652.

[4] P. J. Stephens, F. J. Devlin, C. F. Chabalowski, M. J. Frisch, *The Journal of Physical Chemistry* **1994**, *98*, 11623–11627.

[5] S. Grimme, J. Antony, S. Ehrlich, H. Krieg, *The Journal of Chemical Physics* **2010**, *132*, 154104.

[6] M. Cossi, N. Rega, G. Scalmani, V. Barone, *Journal of Computational Chemistry* **2003**, *24*, 669–681.

[7] M. Krumrey, G. Ulm, *Nuclear Instruments and Methods in Physics Research Section A: Accelerators, Spectrometers, Detectors and Associated Equipment* **2001**, *467-468*, 1175–1178.

[8] A. Hoell, Zizak, I., Bieder, H. & Mokrani, L. German Patent No. DE102006029449, **2007**.

[9] U. Keiderling, *Applied Physics A* **2002**, *74*, s1455–s1457.

[10] I. Bressler, J. Kohlbrecher, A. F. Thunemann, *Journal of Applied Crystallography* **2015**, *48*, 1587–1598.

[11] K. Yan, M. Long, T. Zhang, Z. Wei, H. Chen, S. Yang, et al., *Journal of the American Chemical Society* **2015**, *137*, 4460–4468.

[12] M. A. Flatken, A. Hoell, R. Wendt, E. Härk, A. Dallmann, A. Prause, et al., *Journal of Materials Chemistry A* **2021**, *9*, 13477–13482.

[13] D. Amoroso, G. Nasti, C. M. Sutter-Fella, M. M. Villone, P. L. Maffettone, A. Abate, *Matter* **2024**, *7*, 2399–2430.

[14] T. Maschwitz, L. Merten, F. Ünlü, M. Majewski, F. Haddadi Barzoki, Z. Wu, et al., *Nature Communications* **2025**, *16*, 9894.

[15] E. Radicchi, M. A. Flatken, A. Hoell, E. Mosconi, W. Kaiser, J. Pascual, et al., *Submitted* **2026**.

[16] J. Pascual, G. Nasti, M. H. Aldamasy, J. A. Smith, M. Flatken, N. Phung, et al., *Materials Advances* **2020**, *1*, 1066–1070.